Numerical Modeling of Space Plasma Flows: ASTRONUM-2013
ASP Conference Series, Vol. 488
N. V. Pogorelov, E. Audit, and G. P. Zank, eds.

3D Global Magnetohydrodynamic Simulations of the Solar Wind/Earth's Magnetosphere Interaction

Mehmet Sarp Yalim and Stefaan Poedts

Katholieke Universiteit Leuven, Department of Mathematics,
Center for mathematical Plasma Astrophysics,
Celestijnenlaan 200b - bus 2400, 3001, Leuven, Belgium

Abstract. In this paper, we present results of real-time 3D global magnetohydrodynamic (MHD) simulations of the solar wind interaction with the Earth's magnetosphere using time-varying data from the NASA Advanced Composition Explorer (ACE) satellite during a few big magnetic storm events of the previous and current solar cycles, namely the 06 April 2000, 20 November 2003 and 05 April 2010 storms. We introduce a numerical magnetic storm index and compare the geo-effectiveness of these events in terms of this storm index which is a measure for the resulting global perturbation of the Earth's magnetic field. Steady simulations show that the upstream solar wind plasma parameters enter the low-β switch-on regime for some time intervals during a magnetic storm causing a complex dimpled bow shock structure. We also investigate the traces of such bow shock structures during time-dependent simulations of the events. We utilize a 3D, implicit, parallel, unstructured grid, compressible finite volume ideal MHD solver with an anisotropic grid adaptation technique for the computer simulations.

1. Introduction

Global magnetohydrodynamic (MHD) simulations are important for analyzing and understanding the interaction of the solar wind with the Earth's magnetosphere during magnetic storms. In this paper, we perform global MHD simulations of three magnetic storms of different strengths from the previous and current solar cycles, namely the storms that occurred on 06 April 2000 ($\mathrm{Dst_{min}}$=-288 nT), 20 November 2003 ($\mathrm{Dst_{min}}$ = −472 nT) and 05 April 2010 ($\mathrm{Dst_{min}}$ = −81 nT). We show plots of the interaction between the solar wind and the Earth's magnetosphere, introduce a numerical magnetic storm index, discuss its main features and present an analysis on tracing a complex bow shock structure during a storm.

2. Governing Equations and Numerical Method

In this paper, the $\mathbf{B_0}+\mathbf{B_1}$ splitting technique of Tanaka (1994) is applied to the system of compressible ideal MHD equations modified using the hyperbolic divergence cleaning approach with hyperbolic Lagrange multiplier (Dedner et al. 2002). Accordingly, in non-dimensional, conservative, differential form, this system is given by:

$$\frac{\partial \mathbf{U}}{\partial t} + \nabla \cdot \mathbf{F} = 0, \tag{1}$$

where $\mathbf{U} = \begin{pmatrix} \rho & \rho\mathbf{v} & \mathbf{B}_1 & E_1 & \phi \end{pmatrix}^{\mathrm{T}}$ is the state vector of conservative variables with the flux

$$\mathbf{F} = \begin{pmatrix} \rho\mathbf{v} \\ \rho\mathbf{v}\mathbf{v} + (p + \frac{1}{2}B_1^2 + \mathbf{B_0}\cdot\mathbf{B_1})\mathbf{I} - (\mathbf{B_1}\mathbf{B_1} + \mathbf{B_0}\mathbf{B_1} + \mathbf{B_1}\mathbf{B_0}) \\ \mathbf{v}\mathbf{B} - \mathbf{B}\mathbf{v} + \mathbf{I}\phi \\ \mathbf{v}(E_1 + p + \frac{1}{2}B_1^2 + \mathbf{B_0}\cdot\mathbf{B_1}) - (\mathbf{v}\cdot\mathbf{B_1})\mathbf{B} \\ V_{\mathrm{ref}}^2\mathbf{B_1} \end{pmatrix}. \tag{2}$$

The matrix $\mathbf{I}$ here us a 3×3 identity matrix, $\rho, p, \mathbf{v}, \mathbf{B}$, and $\mathbf{B_1}$ denote the density, thermal pressure, velocity, total magnetic field and variable magnetic field component to be solved, while $\mathbf{B_0}$ represents Earth's dipole magnetic field given by

$$\mathbf{B_0} = \frac{1}{r^3}(3(\mathbf{m}\cdot\mathbf{n_r})\mathbf{n_r} - \mathbf{m}), \tag{3}$$

where $\mathbf{m}$ is the Earth's magnetic dipole moment, $\mathbf{n_r}$ is a unit vector in the $\mathbf{r}$-direction, and r denotes the distance from the center of the dipole chosen as the origin. Furthermore, ϕ, V_{ref} and E_1 are the scalar potential function, a constant reference speed and the specific total energy of the plasma based on $\mathbf{B_1}$, respectively. Finally, there is the solenoidal constraint ($\nabla\cdot\mathbf{B_1} = 0$) which should always be satisfied everywhere in the plasma.

The ideal MHD equations are non-dimensionalized based on the choice of three quantities for the units of length, mass and time (Goedbloed & Poedts 2004). Accordingly, the radius of the Earth, a magnetic field strength of 3.5 nT and the time for the Alfvén waves based on that magnetic field strength and a density of 5 AMU/cm^3 to travel a distance equal to the radius of the Earth are chosen.

The numerical method utilized to discretize the governing equations is an implicit finite volume method which was presented in detail in Yalim et al. (2011). For the simulations performed in this paper, the spatial discretization is made by the second order accurate limited total variation diminishing (TVD) Rusanov scheme using a Barth–Jespersen's limiter. The temporal discretization is made by the standard second order accurate backward differentiation formula (BDF).

3. Results

The computational domain is a rectangular box with dimensions of $-200 \le x \le 235$ and $-50 \le y, z \le 50$ and a sphere of radius 2.5 and center at the origin. The coordinate system utilized is GSM for which the x-axis points at the Sun and the xz-plane contains the dipole axis where a fixed tilt angle of 11.94° is applied. The boundary conditions utilized are superfast inlet and outlet, and ionosphere/magnetosphere interaction. At the superfast inlet which is located at $x = 235$, the solar wind plasma parameters extracted from the 64 s average ACE data are imposed. The superfast outlet is applied to the rest of the box surfaces where the plasma parameters are simply extrapolated to the ghost cells. Finally, at the ionosphere/magnetosphere interaction, the boundary condition suggested in Powell et al. (1999); Gombosi et al. (2002) is applied. Accordingly, the plasma density is fixed to 56 AMU/cm^3 as suggested in Ridley et al. (2010), the temperature is fixed to 35000 K, a no-slip condition is imposed for the velocity and a mirror boundary condition is applied for the perturbation magnetic field.

The 3D unstructured grid we used consists of 473067 nodes and 2773426 tetrahedral elements. It is anisotropically adapted (Majewski & Athanasiadis 2009) once according to the steady state initial solution. Typical cell sizes near the inner boundary, across the bow shock, at the magnetopause, along the magnetotail and at the cusp are 0.15, 0.15, 0.25, 0.2 and 0.2, respectively. In Figure 1, the grid is shown in the xz- and $x = -30$ planes.

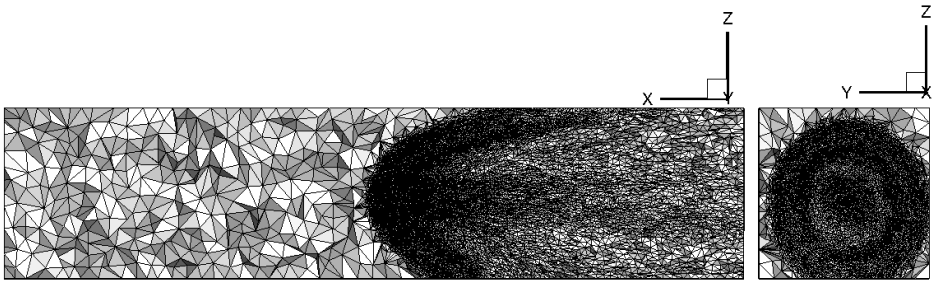

Figure 1. Adapted grid in the xz and $x = -30$ planes.

In Figure 2, magnetic field lines are shown in the vicinity of the Earth at an instant during each storm, i.e. when the B_z component of the interplanetary magnetic field is strongly negative.

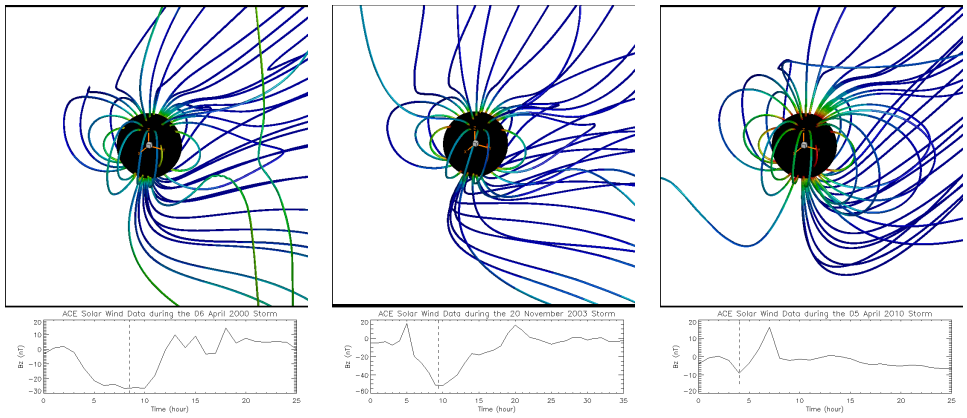

Figure 2. Magnetic field lines in the vicinity of the Earth at an instant during 06 April 2000 (left), 20 November 2003 (middle) and 05 April 2010 (right) storms.

In Figure 3, we present a numerical magnetic storm index based on the average of the magnitude of the perturbation field, $\mathbf{B_1}$, inside a sphere of radius 3 surrounding the Earth. As can be deduced from the variation of the index, the duration of each storm as well as the peak value of the index are proportional to the strength of the storm. Furthermore, for each storm, the times of the initial jump and the peak of the storm index are close to the times of the initial jump and minimum value of the Dst index, respectively.

Complex dimpled bow shock structures can be important in the global reconfiguration of the magnetosheath flow involving a slow shock and thus an increased geoeffectiveness of the storm (De Sterck & Poedts 1999). While such a complex shock

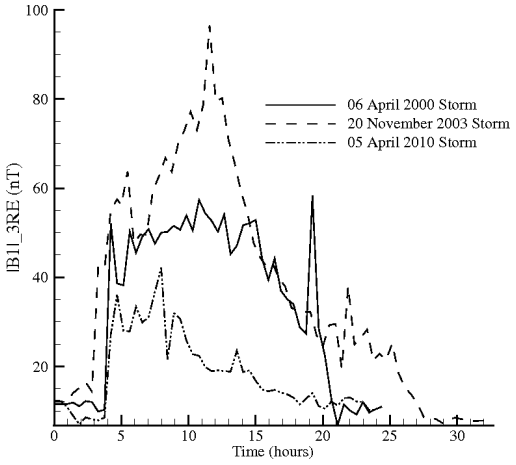

Figure 3. Magnetic storm index variation with time.

structure is obtained when the solar wind plasma parameters are in the low-β switch-on regime for a steady simulation, it is difficult to find a complex shock structure during a real event. According to De Sterck & Poedts (1999), a complex planetary bow shock structure is preferably to occur when $\beta < 2/\gamma$ (in particular for low-β solar wind parameters), the angle between the solar wind velocity and magnetic field, θ_{vB}, is large, the solar wind parameters remain in the magnetically dominated regime for a sufficiently long time, and on the quasi-parallel side of the magnetosheath and not too far from the plane containing the incoming solar wind magnetic field.

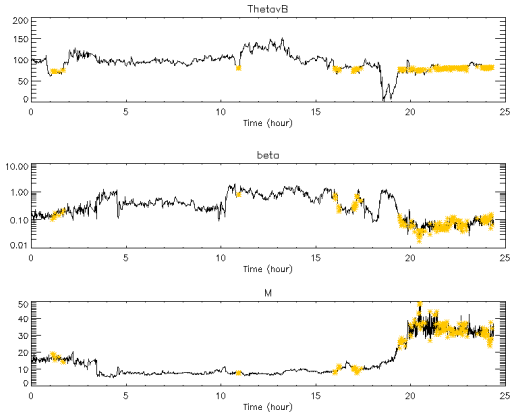

Figure 4. Variations of θ_{vB}, β and Mach number based on the acoustic speed (M) during the 06 April 2000 storm simulation. Instances when the solar wind plasma is in the switch-on regime are indicated with yellow asterisks.

In Figure 4, the instances when the solar wind plasma is in the switch-on regime are shown during the 06 April 2000 storm based on the ACE data. We focus on the relatively long period of switch-on regime at 23 hours. After approximately 40 minutes from the measurement, the related magnetically dominated plasma arrives at the vicinity of the Earth's bow shock. In Figure 5, pressure contours with magnetic field

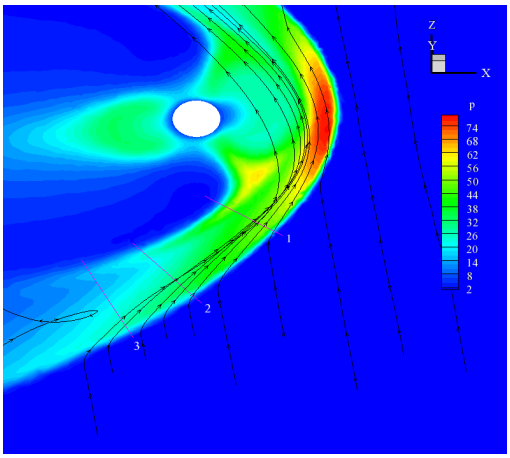

Figure 5. Complex bow shock structure with cuts 1, 2 and 3 for analysis.

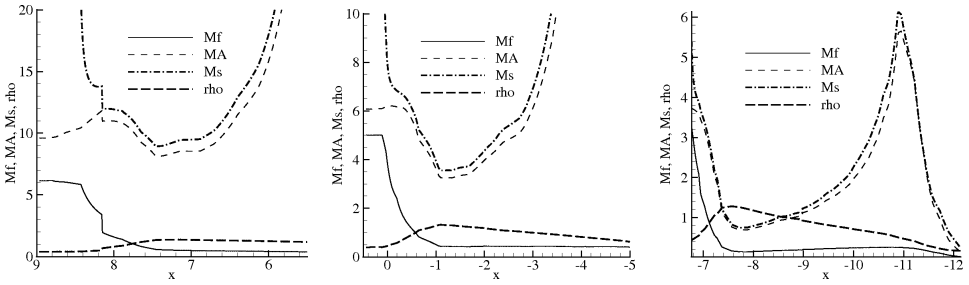

Figure 6. Variations of the Mach numbers based on Alfvén (M_A), fast (M_f) and slow (M_s) magnetoacoustic wave speeds and density across the cuts 1 (left), 2 (middle) and 3 (right).

lines are shown on the plane containing both the solar wind velocity and magnetic field, together with the cuts 1, 2 and 3 for analyzing the shock type. Accordingly, in Figure 6, while going along the shock from the locations of the cut 1 towards the cut 3, the Mach numbers based on the Alfvén and slow magnetoacoustic wave speeds decrease from above to below 1 across the shock. This is an indication of the presence of a complex bow shock structure involving intermediate shocks.

4. Conclusion

In this paper, results of 3D global MHD simulations of the 06 April 2000, 20 November 2003 and 05 April 2010 magnetic storms for which the solar wind plasma parameters at the inlet were extracted from the ACE satellite data are presented. The simulations were performed over anisotropically adapted unstructured grids for which the adaptation was made based on the steady state initial solution. A numerical magnetic storm index is presented based on the average global perturbation of the magnetic field inside the computational domain in the vicinity of the Earth. This index demonstrates the duration of a storm in measure to the strength of the storm. Furthermore, the times when the

initial jump and the peak of the storm index occur are similar to the variations in the Dst index.

Steady simulations show that the bow shock of the Earth can have a complex nature when the solar wind plasma parameters are in the low-β switch-on regime. We also demonstrate the presence of a complex bow shock structure during the time-dependent simulation of the 06 April 2000 magnetic storm.

Finally, the global MHD solver can perform real-time storm simulations with 120 parallel processors. As the parallel scalability of the solver was tested up to 1024 processors, it can also perform such simulations in faster than real time. Furthermore, this solver was implemented inside COOLFluiD, an object-oriented multi-physics framework, which is designed to make the implementation and coupling of different space weather models with the current global MHD model possible. This will be discussed in a future publication.

Acknowledgments. The authors acknowledge the financial support from the C 90347 (ESA PRODEX 10) project and from the projects GOA/2009-009 (KU Leuven) and G.0729.11 (FWO-Vlaanderen). For the simulations, the authors used the infrastructure of the VSC "Flemish Supercomputer Center", funded by the Hercules foundation and the Flemish Government, department EWI. The authors would like to thank Dr. Jurek Majewski, Warsaw University of Technology, Poland for his contribution on grid adaptation. The global MHD solver was developed in the COOLFluiD platform.

References

De Sterck, H., & Poedts, S. 1999, J. Geophys. Res., 104, 22401

Dedner, A., Kemm, F., Kroner, D., Munz, C.-D., Schnitzer, T., & Wesenberg, M. 2002, J. Comp. Phys., 175, 645

Goedbloed, J. P., & Poedts, S. 2004, Principles of Magnetohydrodynamics: With Applications to Laboratory and Astrophysical Plasmas (Cambridge: Cambridge University Press), 1st ed.

Gombosi, T. I., Toth, G., De Zeeuw, D. L., Hansen, K. C., Kabin, K., & Powell, K. G. 2002, J. Comp. Phys., 177, 176

Majewski, J., & Athanasiadis, A. 2009, in Computational Fluid Dynamics 2006: Proceedings of the Fourth International Conference on Computational Fluid Dynamics, edited by H. Deconinck, & E. Dick (Berlin, Heidelberg: Springer Verlag), 389

Powell, K. G., Roe, P. L., Linde, T. J., Gombosi, T. I., & De Zeeuw, D. L. 1999, J. Comp. Phys., 154, 284

Ridley, A. J., Gombosi, T. I., Sokolov, I. V., Toth, G., & Welling, D. T. 2010, Ann. Geophys., 28, 1589

Tanaka, T. 1994, J. Comp. Phys., 111, 381

Yalim, M. S., Vanden Abeele, D., Lani, A., Quintino, T., & Deconinck, H. 2011, J. Comp. Phys., 230, 6136